Journal of Chemical Health Risks

www.jchr.org

JCHR (2025) 15(4),7 01-711 | ISSN:2251-6727

Photocatalytic and Antimicrobial activities of WO_3, $LaWO_3$, and rGO/$LaWO_3$ Nanomaterials for Environmental and Health Applications

Sivarajakrishnan Anandabaskaran, Vijayakumar Uthiravel, Kirusarani Narayanamurthy, Rakshitha Nagappan And Krishnasamy Kuppusamy*.

Corresponding author:- Krishnasamy Kuppusamy

Department of Chemistry, Annamalai University, Annamalai Nagar, Chidambaram - 608 002, Tamil Nadu, India

(Received: 16 May 2025 Revised: 20 June 2025 Accepted: 12 July 2025)

KEYWORDS

Hydrothermal method,

Methylene blue

Photocatalytic study

Antimicrobial applications.

ABSTRACT:

This study is focused on the synthesize of novel rGO/$LaWO_3$ nanocomposite via hydrothermal method and the resulting nanomaterials are thoroughly characterized using several methods, including XRD, FE-SEM, EDS, FT-IR, UV-DRS, HR-TEM, and XPS, to confirm their structural, morphological, and optical properties. XRD analysis reveals average crystallite sizes of 12.85 nm for WO_3, 33.58 nm for $LaWO_3$, and 59.59 nm for the rGO/$LaWO_3$ composite. UV-DRS analysis shows a decrease in the band gap from 1.81 eV for WO_3 to 1.62 eV for rGO/$LaWO_3$. The photocatalytic performance of rGO/$LaWO_3$ nanocomposites is evaluated for the degradation of methylene blue (MB) dye under natural sunlight, achieving significantly higher degradation efficiency than WO_3 and $LaWO_3$. This enhanced photocatalytic performance is attributed to the synergistic effect between rGO and $LaWO_3$, which promotes better charge separation. Kinetic studies confirm a pseudo-first-order reaction mechanism. Additionally, the nanocomposites demonstrate improved antibacterial activity against *S. aureus, E. coli, Salmonella typhi,* and *V. parahaemolyticus*, further confirming their potential for biomedical applications. These findings highlight the potential of rGO/$LaWO_3$ as high-performance photocatalytic and antibacterial nanomaterials, making them strong prospects for wastewater treatment, ecological cleanup, and biomedical uses.

1. Introduction

The escalating concern regarding environmental pollution, particularly the contamination of water resources by synthetic dyes, has necessitated the development of efficient photocatalytic materials that can effectively degrade harmful pollutants. Solar-driven photocatalysis has garnered significant attention among various remediation techniques due to its eco-friendly nature, sustainability, and minimal ecological impact [1]. Tungsten trioxide (WO_3) and its modified derivatives have shown great promise as photocatalysts, owing to their semiconductor properties, chemical stability, and capability to degrade organic dyes when exposed to UV and visible light. WO_3 is a wide band-gap semiconductor with considerable photocatalytic potential, its activity under visible light is hindered by its poor charge carrier mobility and limited performance in the visible light region [2]. To overcome these challenges, doping strategies have been employed to enhance the photocatalytic efficiency of WO_3. One such approach involves doping WO_3 with lanthanide elements (La), such as neodymium (Nd^{3+}), cerium (Ce^{3+}), or europium (Eu^{3+}), which have been found to improve the optical absorption, facilitate charge separation, and increase the surface area of WO_3, thus enhancing its photocatalytic reactivity, particularly under visible light irradiation [3]. In recent years, the integration of WO_3 with reduced graphene oxide (rGO) has been explored as an effective method to further boost photocatalytic efficiency. rGO, with its high surface area, excellent electrical conductivity, and ability to facilitate electron transfer, reduces the recombination of photogenerated electron-hole pairs, leading to enhanced photocatalytic activity for dye degradation. The presence of rGO in WO_3-based composites facilitates better charge separation, resulting in improved photocatalytic performance. The rising global challenge of antimicrobial resistance [4] highlights the need for novel strategies to combat pathogenic microorganisms.

Metal oxide nanoparticles, particularly lanthanum-doped tungsten oxide ($LaWO_3$), have attracted significant attention for their enhanced antimicrobial properties due to their unique physicochemical attributes. Lanthanum-doped WO_3 nanoparticles, including $NdWO_3$, $CeWO_3$, and $EuWO_3$ have demonstrated strong antibacterial activity by generating reactive oxygen species (ROS), such as hydroxyl radicals and superoxide ions, under light exposure [5]. These ROS can disrupt microbial cell structures and lead to bacterial inactivation. WO_3 nanoparticles have shown significant antimicrobial effects against pathogens like *Staphylococcus aureus* and *Escherichia*

Journal of Chemical Health Risks
www.jchr.org
JCHR (2025) 15(4),7 01-711 | ISSN:2251-6727

coli by generating ROS under both UV and visible light exposure [6]. Similarly, other metal oxide nanoparticles like zinc oxide (ZnO), nickel oxide (NiO), and copper(I) oxide (Cu_2O) exhibit similar photocatalytic and antimicrobial behavior, where ROS generation induces oxidative damage to bacterial cells, leading to bacterial death [7]. The incorporation of rGO into metal oxide nanoparticles, including rGO/ZnO, rGO/NiO, rGO/Cu_2O, and rGO/$LaWO_3$, has been shown to enhance the antimicrobial activity of these materials. The addition of rGO improves electrical conductivity, promotes efficient electron transfer, and increases light absorption, thereby boosting photocatalytic efficiency and ROS generation [8]. The synergistic effect between rGO and La-doped WO_3 nanoparticles results in superior antimicrobial performance, particularly against pathogens such as *Salmonella typhi* and *Vibrio parahaemolyticus* [9-10].In this study, WO_3, $LaWO_3$, and rGO/$LaWO_3$ nanoparticles were synthesized using the hydrothermal method. Various characterizations, including XRD, FE-SEM, EDS, FT-IR, UV-DRS, HR-TEM, and XPS, were conducted. The photocatalytic and antimicrobial activities of WO_3, $LaWO_3$, and rGO/$LaWO_3$ were then evaluated, with the results indicating that the rGO/$LaWO_3$ nanoparticles exhibited superior photocatalytic and antimicrobial performance.

2. Experimental

2.1. Materials:

Sodium tungstate, hydrochloric acid, lanthanum (III) chloride, methylene blue, thiourea, and ethanol were obtained from Sigma-Aldrich, and all compounds were used as received without further purification.

2.2. Preparation of Graphene Oxide:

Graphene oxide (GO) was synthesized from graphite powder using a modified Hummer's method. First, 1.0 g of graphite powder and 0.5 g of $NaNO_3$ were mixed into 23 ml of cooled concentrated H_2SO_4. Then, 7.0 g of $KMnO_4$ was gradually added with continuous stirring, maintaining the reaction temperature below 10°C using an ice bath. After 30 minutes, the ice bath was removed, and the mixture was stirred for an additional 30 minutes at 35°C. Subsequently, 46 ml of distilled water was slowly added, raising the temperature to 100°C, and this temperature was maintained for 15 minutes. The reaction was terminated by adding 140 ml of distilled water, followed by 10 ml of a 30% H_2O_2 aqueous solution. The resulting solid was collected by centrifugation and washed repeatedly with 5% HCl solution until sulfate anions were undetectable with $BaCl_2$. The final solid GO was dried under vacuum at 50°C [11].

2.3. Preparation of Reduced Graphene Oxide

Reduced graphene oxide (rGO) was obtained by placing the black powder of GO in a 200 ml beaker. Then, 20 ml of hydrazine hydrate was added, and the mixture was heated on a hot plate at 100°C to 150°C. After 15 minutes, 10 to 15 ml of water was added dropwise to the mixture, and heating continued until the mixture was dry. The dried powder was repeatedly washed and centrifuged with water and acetic acid, and the pH was checked each time to ensure it reached neutrality. The product was collected as reduced graphene oxide (rGO) [12].

2.4. Synthesis of WO_3 Nanoparticles

WO_3 nanoparticles were synthesized using the hydrothermal method. First, 2.63 g of sodium tungstate was dissolved in 60 ml of distilled water, and the solution was stirred for 10 minutes at room temperature in a 250 ml beaker. Following this, 20 ml of concentrated HCl was added dropwise to neutralize the mixture, and then 0.5 g of NaOH, dissolved in 10 ml of water. This addition caused the transparent solution to turn into a yellowish-white precipitate. The mixture was stirred at room temperature for 30 minutes. It was then transferred to a Teflon-lined autoclave and heated to 130°C for 4 hours. After the reaction, the product was washed several times with ethanol and distilled water to purify the tungsten oxide nanoparticles [13]. The obtained product was dried and then calcined at 400°C for 4 hours to yield WO_3 nanoparticles.

2.5. Synthesis of La-doped WO_3 and rGO/$LaWO_3$ Nanocomposites:

Lanthanum-doped WO_3 nanoparticles were synthesized via a hydrothermal method. Initially, 4.12 g of Sodium tungstate were dissolved in 50 ml of distilled water and stirred vigorously to ensure a homogeneous solution. The pH of the solution was then carefully adjusted to approximately 7 using hydrochloric acid. Subsequently, 0.55 g of lanthanum chloride ($LaCl_3$) was added to the solution, followed by 30 minutes of continuous stirring.The resulting solution was transferred to a Teflon-lined autoclave, sealed, and subjected to hydrothermal treatment at 180°C for 12 hours. After cooling to room temperature, the nanoparticles were collected by filtration, washed thoroughly with deionized water and ethanol, and then dried in an oven at 60°C for 12 hours. Finally, the dried nanoparticles were calcined at 400°C for 2 hours to obtain the final lanthanum-doped WO_3 nanoparticles with controlled morphology.

To synthesize rGO/$LaWO_3$ nanoparticles, the procedure described above was followed, with the addition of powdered rGO to the $LaWO_3$ solution before proceeding with the subsequent steps to obtain the composite material [13].

2.6. Photocatalytic Activity

The photocatalytic activity of the synthesized nanomaterials viz., WO_3, $LaWO_3$, and rGO/$LaWO_3$, was evaluated against MB dye under sunlight irradiation [14]. A 20 mg of the nanocatalyst was mixed with 100 mL of 0.3×10^{-4} mol/L MB dye solution, and the mixture was stirred thoroughly. At regular intervals (5 mL every 10 minutes), samples of the

Journal of Chemical Health Risks
www.jchr.org
JCHR (2025) 15(4),7 01-711 | ISSN:2251-6727

sunlight-exposed nanocomposite solutions were taken for absorbance measurement using UV-Vis spectroscopy [15]. The dye degradation efficiency was calculated using the following formula:

$$\text{Degradation efficiency (\%)} = (C_0 - C_t) / C_0 \times 100 \qquad (1)$$

3. Results and Discussion

3.1. X-ray Diffraction (XRD) Analysis

X-ray diffraction (XRD) was employed to investigate the structural and phase properties of reduced graphene oxide (rGO), tungsten trioxide (WO_3), lanthanide-doped tungsten trioxide ($LaWO_3$), and their composite (rGO/$LaWO_3$). The XRD patterns are shown in **Fig. 1.** The XRD pattern of rGO exhibits a broad diffraction peak at approximately $2\theta \approx 26.45°$, corresponding to the (002) plane of graphene oxide. The broadening of this peak indicates a reduction in crystallinity, a characteristic feature of rGO. Additionally, the absence of sharp diffraction peaks confirms its amorphous nature. In contrast, WO_3 displays distinct peaks at 2θ values of 23.5°, 33.2°, 35.3°, 49.4°, and 55.6° corresponding to the monoclinic phase of WO_3 (JCPDS 83-0950), with reflections from the (002), (020), (200), (202), and (222) planes. For La-doped WO_3 ($LaWO_3$), peaks observed at 2θ = 29.04°, 33.66° and 57.40° match the face-centered cubic (FCC) structure (JCPDS 88-2336). This suggests that doping does not significantly alter the phase or crystalline framework of WO_3. The XRD patterns of the rGO/$LaWO_3$ composite exhibits diffraction peaks characteristic of both rGO and $LaWO_3$. The peak at $2\theta \approx 26.45°$ confirms the presence of rGO in the composite, while the well-defined peaks associated with $LaWO_3$ indicate no substantial phase alteration or structural distortion due to composite formation. The crystallite sizes of WO_3, $LaWO_3$, and rGO/$LaWO_3$ were determined using the Debye-Scherrer equation:

$$(D) = \frac{0.9\lambda}{\beta \cos\theta} \qquad (2)$$

where D is the crystallite size, K is a constant (0.9), λ is the X-ray wavelength (1.5406 Å), β is the full width at half maximum (FWHM) of the peak, and θ is the diffraction angle. The calculated average crystallite sizes were 12.85 nm for WO_3, 33.58 nm for $LaWO_3$, and 59.59 nm for the rGO/$LaWO_3$ composite. These results indicate that the composite material exhibits a larger crystallite size compared to its individual components, suggesting that composite formation influences crystal growth behavior.

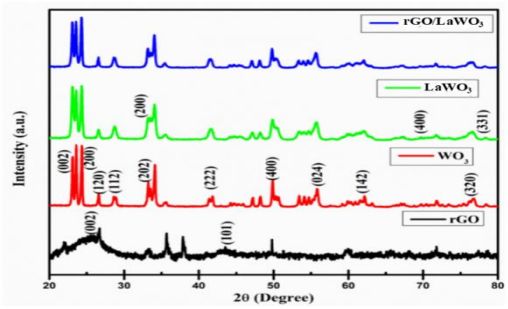

Fig.1. XRD patterns of a) rGO, b) WO_3, c) $LaWO_3$, and d) rGO/$LaWO_3$

3.2. FT-IR Analysis

Fourier-transform infrared (FT-IR) spectroscopy was employed to examine the structural characteristics and bonding interactions of reduced graphene oxide (rGO), tungsten trioxide (WO_3), lanthanum-doped WO_3 (La-doped WO_3), and the rGO/$LaWO_3$ composite, as presented in **(Fig.2a-2d)**. This method effectively identifies the key functional groups and chemical bonds within the materials [17]. The FT-IR spectrum of rGO **(Fig. 2a)** displays a prominent peak at 1631 cm^{-1}, which is associated with the C=C stretching vibration of the graphene sheets. Additionally, a band at 2850 cm^{-1} is observed, corresponding to the C–H stretching vibrations, which suggests the presence of oxygenated functional groups, such as hydroxyl or epoxy, on the surface of rGO [18]. In the case of WO_3 **(Fig.2b)**, a distinct absorption peak at approximately 650 cm^{-1} is observed, corresponding to the W–O stretching vibration, which confirms the presence of tungsten oxide and highlights the characteristic bonding in WO_3.The FT-IR spectrum of La-doped WO_3 **(Fig.2c)** shows a similar W–O stretching vibration around 756 cm^{-1}. However, slight shifts in peak positions and variations in intensity indicate that the doping of lanthanum (La) ions has influenced the local structure and bonding of the WO_3 lattice. These changes suggest a modification of the tungsten oxide framework due to the incorporation of La ions, which alters the electronic environment around the tungsten atoms. For the rGO/$LaWO_3$ composite **(Fig.2d)**, additional peaks corresponding to rGO are evident. The 1631 cm^{-1} band corresponds to the C=C stretching of rGO, while the 2918 cm^{-1} band is attributed to C–H stretching vibrations. The characteristic W–O peaks from both WO_3 and La-doped WO_3 are still observed, suggesting that the tungsten oxide structure remains intact within the composite material [19]. These FT-IR results confirm the successful integration of rGO into the La-doped WO_3 structure, providing strong evidence that the composite maintains the structural integrity of both components. This incorporation likely enhances the photocatalytic properties of the material by promoting a more efficient charge transfer between rGO and the La-doped WO_3, thereby improving overall performance.

Journal of Chemical Health Risks
www.jchr.org
JCHR (2025) 15(4),7 01-711 | ISSN:2251-6727

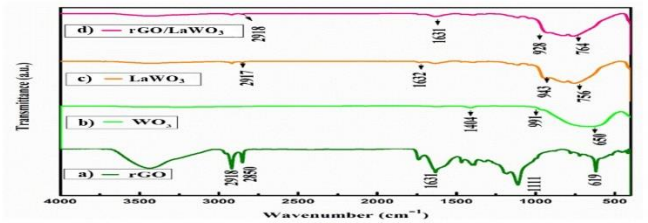

Fig.2. FT-IR spectra of a) rGO, b) WO_3, c) $LaWO_3$, and d) rGO/$LaWO_3$

3.3. UV-DRS Spectra and Tauc Plot Analysis

The UV-DRS spectra of WO_3, La-doped WO_3, and rGO/$LaWO_3$ are shown in **Fig.3a, 3b,** and **3c,** respectively. The UV-DRS spectrum of WO_3 exhibits strong absorption in the ultraviolet (UV) region, with a band gap of 1.81 eV, which is characteristic of tungsten oxide's electronic transitions [13]. For La-doped WO_3, the absorption spectrum shows a slight redshift, Indicating a narrowing of the band gap to approximately 1.74 eV. This reduction in band gap is attributed to the incorporation of lanthanum ions, which alter the electronic properties of WO_3, enhancing light absorption and potentially improving photocatalytic performance under visible light [20]. The UV-DRS spectrum of the rGO/$LaWO_3$ composite displays further enhancement in absorption across a broader wavelength range, with the estimated band gap reduced to 1.62 eV. This additional band gap reduction can be attributed to the synergistic effect of lanthanum doping and the presence of reduced graphene oxide (rGO). The rGO component facilitates efficient charge transfer, contributing to enhanced photocatalytic performance by promoting better visible-light absorption [21]. The corresponding Tauc plots for WO_3, La-doped WO_3, and rGO/$LaWO_3$ were obtained by plotting $(\alpha h\nu)^2$ versus photon energy ($h\nu$), as shown in **Fig. 4.** The linear regions of these plots were extrapolated to the x-axis to determine the respective band gap values [16]. The Tauc plots confirmed the band gap values obtained from UV-DRS spectra, with WO_3, La-doped WO_3, and rGO/$LaWO_3$ exhibiting band gaps of 1.81 eV, 1.74 eV, and 1.62 eV, respectively. These findings highlight the effectiveness of lanthanum doping and rGO incorporation in narrowing the band gap, which could significantly improve photocatalytic activity under visible light.

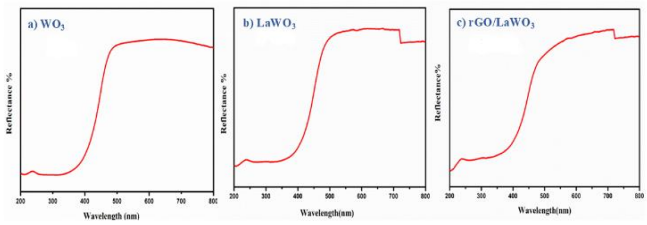

Fig.3. UV-DRS spectrum of a) WO_3, b) $LaWO_3$, and c) rGO/$LaWO_3$

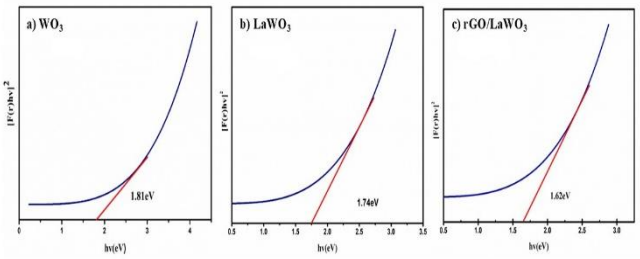

Fig.4. Tauc plot of a) WO_3, b) $LaWO_3$, and c) rGO/$LaWO_3$

3.4. FE-SEM and EDS Characterization

The FE-SEM images and EDS spectra of the synthesized nanomaterials viz., rGO, WO_3, La-doped WO_3, and rGO/$LaWO_3$, are displayed in **Figures 5** and **6.** Each material exhibits distinct morphological characteristics. The FE-SEM image of rGO **(Fig. 5a)** displays a sheet-like structure, which is a characteristic feature of reduced graphene oxide [22]. In contrast, WO_3 **(Fig. 5b)** consists of aggregated particles, a typical morphology observed in tungsten oxide materials. The La-doped WO_3 **(Fig. 5c)** exhibits a similar agglomerated morphology, with slight variations in particle size and distribution, likely due to lanthanum ion (La) doping. This doping affects particle arrangement and local bonding within the WO_3 framework. In the rGO/$LaWO_3$ composite **(Fig. 5d),** La-doped WO_3 particles are uniformly dispersed on the surface of the rGO sheets. This even distribution confirms the successful integration of La-doped WO_3 onto rGO, which enhances photocatalytic activity by improving charge transfer interactions between the components.

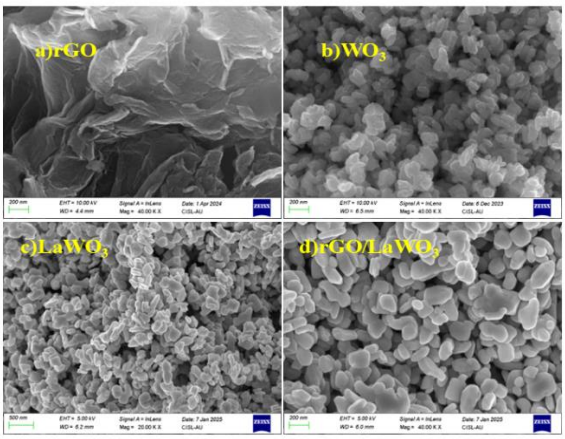

Fig.5. FE-SEM surface morphology analysis of) rGO, b) WO_3, c) $LaWO_3$ and d) rGO/$LaWO_3$

The elemental composition of the materials was further analyzed using EDS. The EDS spectra **(Fig. 6)** confirm the presence of the expected elements in each sample. The rGO spectrum exhibits a peak corresponding to carbon (C) [23], while the WO_3 and La-doped WO_3 samples show peaks for tungsten (W), oxygen (O), and lanthanum (La). The EDS spectrum of the rGO/$LaWO_3$

Journal of Chemical Health Risks
www.jchr.org
JCHR (2025) 15(4),7 01-711 | ISSN:2251-6727

composite displays peaks for carbon, tungsten, oxygen, and lanthanum, validating the successful synthesis of the composite material.

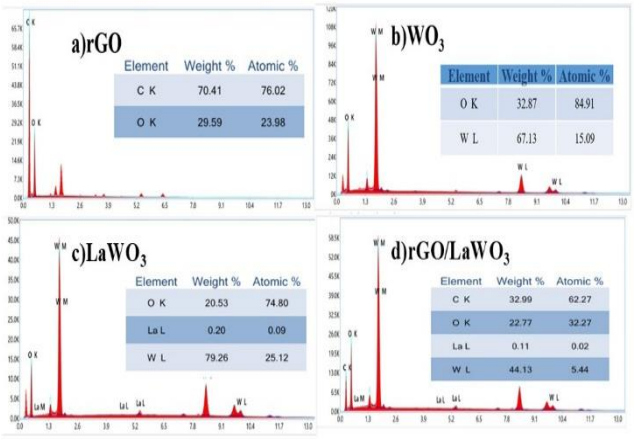

Fig.6. EDX analysis of a) rGO, b) WO_3, c) $LaWO_3$, and d) rGO/$LaWO_3$

3.5. HR-TEM Analysis of rGO/$LaWO_3$ Composite

The high-resolution transmission electron microscopy (HR-TEM) images **(Fig. 7a & 7b)** of the rGO/$LaWO_3$ composite reveal distinct structural features, confirming the successful integration of reduced graphene oxide (rGO) [24] and lanthanum-doped tungsten oxide. The rGO sheets exhibit a characteristic layered structure, acting as an effective scaffold for the uniform dispersion of $LaWO_3$ nanoparticles. This uniform dispersion prevents particle agglomeration and enhances interfacial interactions between rGO and La-doped tungsten oxide, which is crucial for improving electronic conductivity and facilitating efficient charge separation both essential for enhanced photocatalytic performance [25]. The high-resolution lattice images **(Fig. 7c)** display well-defined lattice fringes with spacings of 1.85 nm, 2.64 nm, and 2.66 nm, corresponding to the (220), (104), and (200) crystal planes of $LaWO_3$. These interplanar distances confirm the high crystallinity of the material. The presence of well-ordered lattice fringes indicates that the $LaWO_3$ nanoparticles possess a highly crystalline structure, which is essential for efficient electron transport and charge carrier migration which is a key factor for enhancing photocatalytic efficiency. Further confirmation of the crystalline nature of the rGO/$LaWO_3$ composite is provided by the Selected Area Electron Diffraction (SAED) patterns **(Fig. 7d).** The SAED patterns exhibit distinct diffraction spots that correspond to the $LaWO_3$ phase, reinforcing the conclusion that the composite retains a high degree of crystallinity, which is vital for optimizing photocatalytic activity [26]. The sharp diffraction patterns further suggest that the rGO and $LaWO_3$ phases are well-aligned, contributing to the enhanced stability and overall performance of the material.

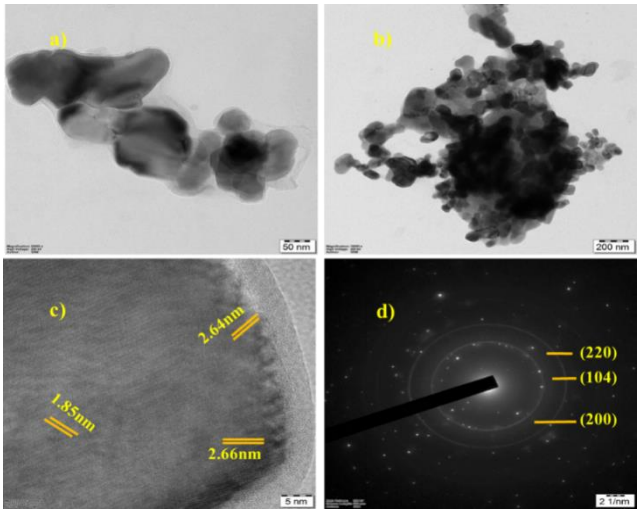

Fig.7. HR - TEM image of lattice fringes and SAED patterns of rGO/$LaWO_3$

3.6. XPS Analysis

X-ray photoelectron spectroscopy (XPS) was conducted to analyze the surface elemental composition and oxidation states of the elements in the rGO/$LaWO_3$ composite, as shown in **Fig. 8.** The survey spectrum of rGO/$LaWO_3$ was recorded over a binding energy range of 0 to 1200 eV, identifying the presence of key elements: carbon (C), oxygen (O), tungsten (W), and the lanthanum (La). This confirms the successful formation of the composite [22]. The W 4f spectrum of rGO/$LaWO_3$ exhibits two prominent peaks at approximately 35.7 eV and 37.8 eV, corresponding to the W $4f_{7/2}$ and W $4f_{5/2}$ binding energies, respectively [27]. These peaks are characteristic of the W^{6+} oxidation state, indicating that the tungsten oxide phase remains stable within the composite. The O 1s spectrum shows a strong peak around 530 eV, which is typically associated with oxygen atoms bonded to tungsten in WO_3, confirming the presence of oxygen within the lattice structure [28]. The C 1s spectrum features a prominent peak at 285.03 eV, attributed to C–C bonds in the rGO sheets [29]. This confirms the incorporation of reduced graphene oxide in the composite and suggests effective integration of rGO with the La-doped WO_3 matrix. For the lanthanum element (La), distinct peaks are observed at 836.5 eV and 852.3 eV, corresponding to the La $3d_{5/2}$ and La $3d_{3/2}$ states of the lanthanum used for doping WO_3. These peaks confirm the successful doping process, and the binding energy values further support the incorporation of lanthanum into the composite. Overall, the XPS analysis provides a comprehensive understanding of the elemental composition and chemical states of the surface components in the rGO/$LaWO_3$ composite. The results confirm the successful integration of rGO with La-doped WO_3, indicating that the composite maintains the structural integrity of WO_3 while

Journal of Chemical Health Risks
www.jchr.org
JCHR (2025) 15(4),7 01-711 | ISSN:2251-6727

benefiting from enhanced electronic and structural properties introduced by the lanthanum dopant.

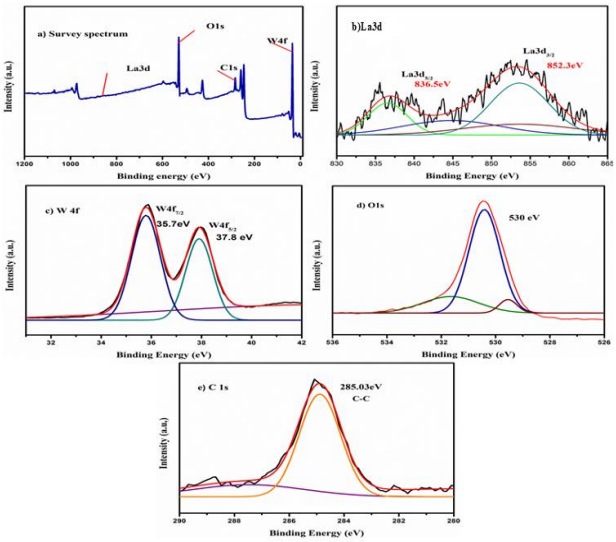

Fig.8. X-ray photoelectron spectroscopy analysis of rGO/$LaWO_3$

3.7. Photocatalytic Activity

Recent studies have demonstrated the effective photocatalytic degradation of methylene blue (MB) dye under natural sunlight using various photocatalysts [30]. These include tungsten oxide (WO_3), lanthanum-doped WO_3 (La-doped WO_3), and reduced graphene oxide (rGO) integrated with La-doped WO_3 (rGO/$LaWO_3$) composites, as illustrated in **Fig. 9** [31]. The synthesized photocatalysts exhibited varying degradation efficiencies: WO_3 (59.4%), La-doped WO_3 (74.5%), and rGO/$LaWO_3$ (92.8%), with a catalyst concentration of 20 mg/mL. WO_3 alone displayed moderate photocatalytic activity, achieving a degradation efficiency of 59.4%. This performance is attributed to its adequate surface area and light absorption properties [32]. However, its relatively low charge carrier separation efficiency limits its overall photocatalytic effectiveness. The incorporation of lanthanum (La) elements into WO_3 (La-doped WO_3) significantly enhanced the photocatalytic efficiency, increasing the degradation rate to 74.5%. Lanthanum doping improves charge carrier separation, broadens the absorption spectrum, and introduces additional active sites, all of which contribute to a more efficient photocatalytic degradation process [33]. Further enhancement was observed with the addition of reduced graphene oxide (rGO) to La-doped WO_3, resulting in an even higher photocatalytic activity. The rGO/$LaWO_3$ composite achieved an impressive degradation efficiency of 92.8%. The rGO component acts as an efficient electron sink, reducing charge carrier recombination and facilitating electron-hole migration to the surface for redox reactions. Additionally, rGO enhances overall charge transfer, increases the number of active sites, and significantly improves photocatalytic performance under sunlight [34]. This synergistic combination of rGO and La-doped WO_3 results in a highly efficient photocatalyst for MB dye degradation under natural sunlight.

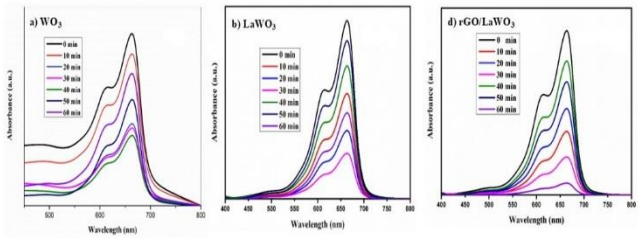

Fig.9. Photocatalytic degradation of a) WO_3, b) La-doped WO_3 and c) rGO/$LaWO_3$

A clear linear relationship between $\ln(C_0/C_t)$ and time was observed, confirming that the degradation process follows pseudo-first-order kinetics, as shown in **Fig. 10.** The calculated rate constants for WO_3, $LaWO_3$, and rGO/$LaWO_3$ were 1.36×10^{-4} min^{-1} , 1.71×10^{-4} min^{-1} and 2.13×10^{-4} min^{-1} respectively. Notably, rGO/$LaWO_3$ exhibited the highest rate constant, indicating its superior photocatalytic performance. These results highlight the synergistic effect of rGO and lanthanide doping in enhancing the photocatalytic degradation of MB dye. The photocatalytic degradation process occurs when WO_3, $LaWO_3$, and rGO/$LaWO_3$ nanoparticles absorb light energy equal to or greater than their bandgap, exciting electrons (e^-) from the valence band (VB) to the conduction band (CB) and generating electron-hole pairs (e^-/h^+). The photogenerated electrons reduce oxygen molecules, forming superoxide radicals ($O_2\bullet^-$), while the holes oxidize water to produce hydroxyl radicals (•OH). These reactive species, particularly hydroxyl radicals, play a crucial role in degrading organic pollutants such as MB dye, breaking them down into non-toxic byproducts. The degradation of MB dye primarily occurs through oxidation by hydroxyl radicals and superoxide anion radicals, as demonstrated by the following mechanism [35].

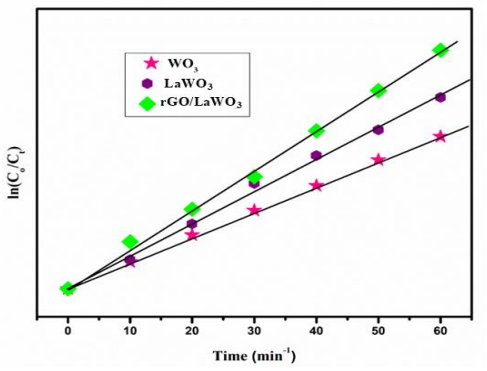

Fig.10. Pseudo-first order plot of a) WO_3, b) La-doped WO_3 and c) rGO/$LaWO_3$

Journal of Chemical Health Risks
www.jchr.org
JCHR (2025) 15(4),7 01-711 | ISSN:2251-6727

In these reactions, hydroxyl radicals (•OH) and superoxide radicals ($O_2^{\bullet-}$) are pivotal in the degradation of MB dye [36], facilitating its breakdown into environmentally benign byproducts such as CO_2 and H_2O. The rGO/$LaWO_3$ composite, combining the electron-accepting characteristics of rGO with the enhanced charge separation facilitated by lanthanum doping, serves as a highly efficient photocatalyst for the degradation of organic pollutants when exposed to natural sunlight.

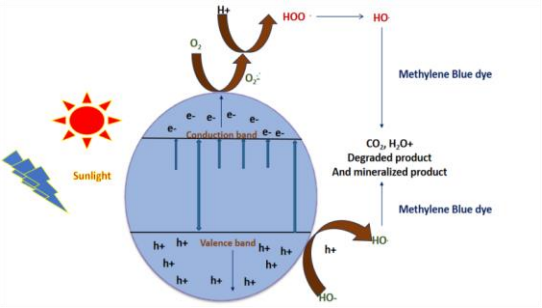

Fig.11. Schematic illustration of the photocatalytic degradation mechanism

3.8. Antibacterial Activity

The antibacterial properties of WO_3, $LaWO_3$, and rGO/$LaWO_3$ nanomaterials were assessed against a range of Gram-negative and Gram-positive bacterial strains at varying concentrations (250 µg/ml, 500 µg/ml, and 1000 µg/ml) using the disc diffusion method [37]. Ampicillin was used as the standard antibiotic for comparison [38]. All three nanomaterials exhibited notable antibacterial activity against all tested strains. As shown in **Fig. 12** and summarized in **Table 1,** WO_3 nanoparticles demonstrated concentration-dependent inhibition across all bacterial species [38]. The most significant inhibition was observed against *Vibrio parahaemolyticus* (15 mm at 1000 µg/ml), which was comparable to the inhibition zone of Ampicillin (16 mm) for the same bacterium. As depicted in **Fig. 13** and summarized in **Table 2,** $LaWO_3$ nanoparticles also exhibited concentration-dependent antibacterial activity. Notably, $LaWO_3$ displayed a similar zone of inhibition against *Escherichia coli* (9 mm for $LaWO_3$ vs. 10 mm for Ampicillin). The highest inhibition by $LaWO_3$ was recorded against *V. parahaemolyticus* (14 mm at 1000 µg/ml). In contrast, as shown in **Fig. 13** and summarized in **Table 3**, the rGO/$LaWO_3$ nanocomposite demonstrated the most potent antibacterial effect overall, showing concentration-dependent inhibition against all bacterial strains. Notably, rGO/$LaWO_3$ exhibited a zone of inhibition against *E. coli* (7 mm) that was slightly lower than that of Ampicillin (10 mm). The maximum inhibition was observed against *V. parahaemolyticus* (15 mm at 1000 µg/ml). The antibacterial activity of these nanomaterials can be attributed to several mechanisms. The positively charged surface of the materials can interact with the negatively charged bacterial cell membranes, leading to membrane destabilization. Additionally, upon exposure to light or other stimuli, these nanomaterials can generate reactive oxygen species (ROS) [39], which can damage cellular structures such as proteins, lipids, and DNA, ultimately leading to bacterial cell death. Overall, the results demonstrate that WO_3, $LaWO_3$, and rGO/$LaWO_3$ nanomaterials possess significant antibacterial activity against a broad spectrum of bacterial strains. $LaWO_3$ and rGO/$LaWO_3$ exhibited the most promising results, with rGO/$LaWO_3$ showing enhanced activity compared to WO_3. The improved antibacterial performance of rGO/$LaWO_3$ relative to pristine WO_3 and $LaWO_3$ is likely attributable to synergistic effects between the components [40].

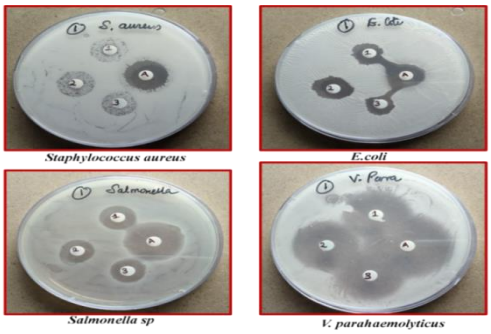

Fig.12. Antibacterial activity of WO_3

S. No	Organism	Zone of inhibition (mm) Concentration (µg/ml)			Standard (Ampicillin)
		1000	500	250	
1	*S. aureus*	9	9	8	11
2	*E. coli*	6	6	5	10
3	*Salmonella typhi*	7	6	6	13
4	*Vibrio parahaemolyticus*	15	14	14	16

Table.1. Antibacterial activity of WO_3

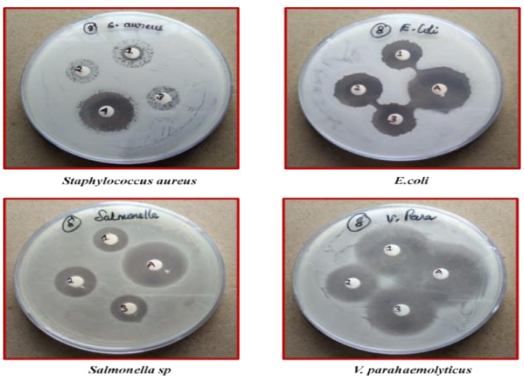

Fig.13. Antibacterial activity of $LaWO_3$

Journal of Chemical Health Risks
www.jchr.org
JCHR (2025) 15(4),7 01-711 | ISSN:2251-6727

S. No	Organism	Zone of inhibition (mm)			Standard (Ampicillin)
		Concentration (µg/ml)			
		1000	500	250	
1	*S. aureus*	10	7	6	11
2	*E. coli*	9	8	8	10
3	*Salmonella typhi*	9	7	6	13
4	*Vibrio parahaemolyticus*	14	13	11	16

Table.2. Antibacterial activity of $LaWO_3$

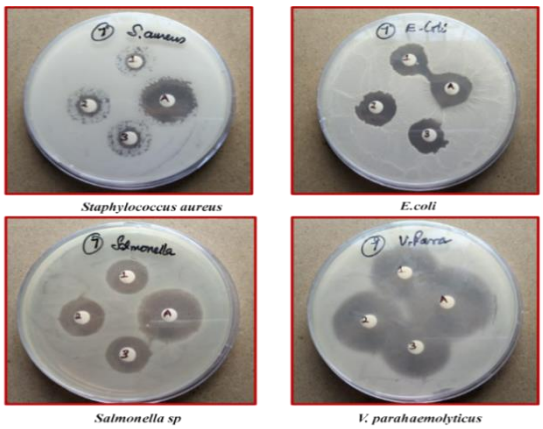

Fig.14. Antibacterial activity of $rGO/LaWO_3$

S. No	Organism	Zone of inhibition (mm)			Standard (Ampicillin)
		Concentration (µg/ml)			
		1000	500	250	
1	*S. aureus*	10	9	9	11
2	*E. coli*	7	7	6	10
3	*Salmonella typhi*	9	9	7	13
4	*Vibrio parahaemolyticus*	15	13	11	16

Table.3. Antibacterial activity of $rGO/LaWO_3$

Conclusion

This study explores the synthesis and characterization of tungsten trioxide (WO_3), lanthanum-doped tungsten trioxide ($LaWO_3$, with neodymium as the dopant), and reduced graphene oxide/lanthanum-doped tungsten trioxide ($rGO/LaWO_3$) composites via the hydrothermal method. The study evaluates their photocatalytic performance in the degradation of methylene blue (MB) dye under natural sunlight. The synthesized materials were thoroughly characterized using various techniques, including XRD, FE-SEM, EDAX, FT-IR, UV-DRS, HR-TEM, and XPS. XRD analysis confirmed the monoclinic and hexagonal structures of WO_3 and $LaWO_3$, respectively, while the $rGO/LaWO_3$ composite maintained the crystallinity of both components. UV-DRS measurements revealed a reduction in the band gap from 1.81 eV for WO_3 to 1.62 eV for $rGO/LaWO_3$ result in enhancing its photocatalytic efficiency. The presence of rGO facilitated better dispersion of $LaWO_3$ nanoparticles, forming a conductive network that improved charge transfer. Photocatalytic tests showed that $rGO/LaWO_3$ exhibited superior methylene blue degradation (92.8%), outperforming both WO_3 (59.4%) and $LaWO_3$ (74.5%). This enhanced performance is attributed to the synergistic interaction between rGO and $LaWO_3$, which promotes effective charge separation and electron transfer. The degradation process followed pseudo-first-order kinetics, with the highest rate constant observed for $rGO/LaWO_3$ (2.13×10^{-4} min^{-1}). Additionally, $rGO/LaWO_3$ demonstrated improved antibacterial activity against common pathogens such as *S. aureus*, *E. coli*, *Salmonella typhi*, and *Vibrio parahaemolyticus*, suggesting its promising potential in antimicrobial applications. These results indicate that $rGO/LaWO_3$ holds significant potential for photocatalytic and microbial applications leading to the environmental and health remediations.

References:

[1] Dhanraj, G., O. Raina, M. Surendar, S. Gopinath, M. Aslam Manthrammel, and Mohd Shkir. "Stable and cost-effective La-doped WO_3 nanoparticles for photocatalytic degradation of organic and antibiotic pollutants under visible light." *Ceramics International* (2025).

[2] Tiwari, Manjula, and G. C. Joshi. "Starch-assisted precipitation synthesis of molybdenum-doped WO_3 nanoparticles for degradation of crystal violet and rhodamine-B dye under direct sunlight irradiation." *Journal of Sol-Gel Science and Technology* (2024): 1-20.

[3] Tahir, M. Bilal, Ghulam Nabi, N. R. Khalid, and M. Rafique. "Role of europium on WO_3 performance under visible-light for photocatalytic activity." *Ceramics International* 44, no. 5 (2018): 5705-5709.

[4] Alsafari, Ibrahim A., Khadija Chaudhary, Muhammad Farooq Warsi, Al-Zoha Warsi, Muhammad Waqas,

Journal of Chemical Health Risks

www.jchr.org

JCHR (2025) 15(4),7 01-711 | ISSN:2251-6727

Murtaza Hasan, Akmal Jamil, and Muhammad Shahid. "A facile strategy to fabricate ternary WO_3/CuO/rGO nano-composite for the enhanced photocatalytic degradation of multiple organic pollutants and antimicrobial activity." *Journal of Alloys and Compounds* 938 (2023): 168537.

[5] Habtemariam, Asratemedhin B., and Yihun Alemu. "Synthesis of WO3 nanoparticles using Rhamnus prinoides leaf extract and evaluation of its antibacterial activities." *Biointerface Res. Appl. Chem* 12, no. 1 (2021): 529-536.

[6] Barbhuiya, Monjur Hassan, Dona Mazumder, Piyush Pandey, and Siddhartha Sankar Dhar. "WO_3@ Bi_2O_3 nanocomposite decorated on N-rGO sheets: A convenient approach to synthesis, characterization, and analysis of their antibacterial behaviour." *Inorganic Chemistry Communications* 173 (2025): 113842.

[7] Bashir, Arslan, Shanza Rauf Khan, Amjad Islam Aqib, Laiba Shafique, and Farid S. Ataya. "Multifunctional integration of tungsten oxide (WO_3) coating: A versatile approach for enhanced performance of antibiotics against single mixed bacterial infections." *Microbial Pathogenesis* 189 (2024): 106571.

[8] Muniyalakshmi, M., C. Anantha Prabhu, D. Thilaga Sundari, R. Sarika, D. Silambarasan, and V. Prasanna Venkatesh. "Synthesis and characterization of WO_3-GO nanocomposite for hydrogen storage, electrochemical, antibacterial and anticancer applications." *Solid State Sciences* 158 (2024): 107764.

[9] Thirumoorthi, G., B. Gnanavel, M. Kalaivani, Abirami Ragunathan, and Hariharan Venkatesan. "Suitability of iron (Fe)-doped tungsten oxide (WO_3) nanomaterials for photocatalytic and antibacterial applications." *International Journal of Nanoscience* 20, no. 05 (2021): 2150042.

[10] Nguyen, Khoa Dang, Nguyen Quang Thinh Le, Linh Tieu Loan Tieu, Thuy Huong Nguyen, Thi Lan Anh Luu, Huu Hung Nguyen, Cong Tu Nguyen, and Ngoc Phuong Thao Nguyen. "Facile one-step synthesis of in situ WO_3@ Gr nanorods as an efficient material for antimicrobial and decoloration applications." *Advances in Natural Sciences: Nanoscience and Nanotechnology* 15, no. 2 (2024): 025009.

[11] Zhu, Xiying, Pan Zhang, Bin Li, Qun Hu, Wenli Su, Lihui Dong, and Fan Wang. "Preparation, characterization and photocatalytic properties of La/WO_3 composites." *Journal of Materials Science: Materials in Electronics* 28 (2017): 12158-12167.

[12] Jamila, Ghulam Sughra, Shamaila Sajjad, Sajjad Ahmed Khan Leghari, and Mingce Long. "Nitrogen doped carbon quantum dots and GO modified WO_3 nanosheets combination as an effective visible photo catalyst." *Journal of hazardous materials* 382 (2020): 121087.

[13] Adhikari, Sangeeta, K. Sarath Chandra, Do-Heyoung Kim, Giridhar Madras, and Debasish Sarkar. "Understanding the morphological effects of WO_3 photocatalysts for the degradation of organic pollutants." *Advanced Powder Technology* 29, no. 7 (2018): 1591-1600.

[14] Dong, Pengyu, Guihua Hou, Xinguo Xi, Rong Shao, and Fan Dong. "WO_3-based photocatalysts: morphology control, activity enhancement and multifunctional applications." *Environmental Science: Nano* 4, no. 3 (2017): 539-557.

[15] Samuel, Ojo, Mohd Hafiz Dzarfan Othman, Roziana Kamaludin, Oulavanh Sinsamphanh, Huda Abdullah, Mohd Hafiz Puteh, and Tonni Agustiono Kurniawan. "WO_3–based photocatalysts: A review on synthesis, performance enhancement and photocatalytic memory for environmental applications." *Ceramics International* 48, no. 5 (2022): 5845-5875.

[16] Jeyapaul, T., K. Prakash, S. Harikengaram, A. Chellamani, and V. Selvam. "Synthesis of WO_3 nanorods and their photocatalytic degradation of organic contaminants." *Rasayan J. Chem* 11, no. 4 (2018): 1405-1414.

[17] Uthiravel, Vijayakumar, Kirusarani Narayanamurthi, Vasanth Raja, Sivarajakrishnan Anandhabasker, and Krishnasamy Kuppusamy. "Green synthesis and characterization of TiO_2 and Ag-doped TiO_2 nanoparticles for photocatalytic and antimicrobial applications." *Inorganic Chemistry Communications* 170 (2024): 113327.

[18] Faris, Abbas Hasan, Khaled J. Hamid, Amel Muhson Naji, Mustafa KA Mohammed, Olfat A. Nief, and Majid S. Jabir. "Novel Mo-doped WO_3/ZnO nanocomposites loaded with polyvinyl alcohol towards efficient visible-light-driven photodegradation of methyl orange." *Materials Letters* 334 (2023): 133746.

[19] Tahir, Muhammad Bilal, Muhammad Sagir, M. Zubair, M. Rafique, Ifra Abbas, M. Shakil, Isa Khan, S. Afsheen, A. Hasan, and Adeel Ahmed. "WO_3 nanostructures-based photocatalyst approach towards degradation of RhB dye." *Journal of Inorganic and Organometallic Polymers and Materials* 28 (2018): 1107-1113.

[20] Govindaraj, T., C. Mahendran, V. S. Manikandan, and R. Suresh. "One-pot synthesis of tungsten oxide nanostructured for enhanced photocatalytic organic dye

degradation." *Journal of Materials Science: Materials in Electronics* 31 (2020): 17535-17549.

[21] Kuriakose, Soumya, H. Hitha, Anjaly Jose, Mathew John, and Thomas Varghese. "Structural and optical characterization of lanthanum tungstate nanoparticles synthesized by chemical precipitation route and their photocatalytic activity." *Optical Materials* 99 (2020): 109571.

[22] Khan, MA Majeed, Manjeet Pawar, Anees A. Ansari, Maqusood Ahamed, Sushil Kumar, and Mohammed Shahabuddin. "Boosted photocatalytic and electrochemical activity of hydrothermally synthesized WO_3 nanoparticles co-doped with transition elements (Mn, Co)." *Materials Science and Engineering: B* 307 (2024): 117541.

[23] Hu, Xiaoxiao, Peiquan Xu, Hongying Gong, and Guotao Yin. "Synthesis and characterization of WO_3/graphene nanocomposites for enhanced photocatalytic activities by one-step in-situ hydrothermal reaction." *Materials* 11, no. 1 (2018): 147.

[24] Taneja, Pankaj, Shelja Sharma, Ahmad Umar, Surinder Kumar Mehta, Alex O. Ibhadon, and Sushil Kumar Kansal. "Visible-light driven photocatalytic degradation of brilliant green dye based on cobalt tungstate ($CoWO_4$) nanoparticles." *Materials Chemistry and Physics* 211 (2018): 335-342.

[25] Karthikeyan, Subramani, Ponnusamy Sasikumar, Jayachandhiran Arumugam, Mohamad Abd E. Abbas, and Subramanian Nithiyanantham. "Morphological and optical investigation of Ce doped La_2O_3 nanoparticles for photocatalytic applications." *Vietnam Journal of Chemistry* (2024).

[26] Abbaspoor, Mahboobeh, Maryam Aliannezhadi, and Fatemeh Shariatmadar Tehrani. "High-performance photocatalytic WO_3 nanoparticles for treatment of acidic wastewater." *Journal of Sol-Gel Science and Technology* 105, no. 2 (2023): 565-576.

[27] Kumaravel, Sakthivel, Sivakumar Thiripuranthagan, Thanigaivel Vembuli, Elangovan Erusappan, Mathivanan Durai, Thamaraiselvi Sureshkumar, and Mani Durai. "Fabrication of mesoporous WO_3-SBA-15 catalysts and enhanced photocatalytic degradation of harmful dyes." *Optik* 235 (2021): 166599.

[28] Ghattavi, Shirin, and Alireza Nezamzadeh-Ejhieh. "A double-Z-scheme ZnO/AgI/WO_3 photocatalyst with high visible light activity: experimental design and mechanism pathway in the degradation of methylene blue." *Journal of Molecular Liquids* 322 (2021): 114563.

[29] Thiyagarajan, Thilagavathi, Venugopal Deivasigamani, Marnadu Raj, Chandrasekaran Joseph, Thangaraju Dheivasigamani, Baskaran Palanivel, Mohamed S. Hamdy, and Mohd Shkir. "Facile synthesis and characterization of WO_3/$CuWO_4$ nanocomposites for the removal of toxic methylene blue dye." *Korean Journal of Chemical Engineering* 38, no. 5 (2021): 952-965.

[30] Younas, Umer, Awais Ahmad, Aftab Islam, Faisal Ali, Muhammad Pervaiz, Aimon Saleem, Muhammad Waseem, Ahmed Muteb Aljuwayid, Mohamed A. Habila, and Salman Raza Naqvi. "Fabrication of a novel nanocomposite (TiO_2/WO_3/V_2O_5) by hydrothermal method as catalyst for hazardous waste treatment." *Fuel* 349 (2023): 128668.

[31] Samuel, Ojo, Mohd Hafiz Dzarfan Othman, Roziana Kamaludin, Oulavanh Sinsamphanh, Huda Abdullah, Mohd Hafiz Puteh, and Tonni Agustiono Kurniawan. "WO_3–based photocatalysts: A review on synthesis, performance enhancement and photocatalytic memory for environmental applications." *Ceramics International* 48, no. 5 (2022): 5845-5875.

[32] Govindaraj, T., C. Mahendran, V. S. Manikandan, J. Archana, Mohd Shkir, and J. Chandrasekaran. "Fabrication of WO_3 nanorods/RGO hybrid nanostructures for enhanced visible-light-driven photocatalytic degradation of Ciprofloxacin and Rhodamine B in an ecosystem." *Journal of Alloys and Compounds* 868 (2021): 159091.

[33] Aldrees, Ali, Hayat Khan, Abdulaziz Alzahrani, and Salisu Dan'azumi. "Synthesis and characterization of tungsten trioxide (WO." (2023).

[34] Sharifiyan, Maryam Sadat, Arash Fattah-alhosseini, and Minoo Karbasi. "Photocatalytic evaluation of hierarchical TiO_2/WO_3 hybrid coating created by PEO/hydrothermal method." *Applied Surface Science Advances* 18 (2023): 100541.

[35] Waheed, Zainab, Sadia Ghazanfar, Muhamamd Usman, Hafiz Muhammad Asif, Muhammad Tariq, Khalid Mahmood, Ali Haider, and Muhammad Sirajuddin. "Synthesis and characterization of ternary composite g-C_3N_4-WO_3/rGO for photocatalytic activity in degradation of methylene blue." *Bulletin of the Chemical Society of Ethiopia* 37, no. 5 (2023): 1123-1131.

[36] Nguyen, Tien Anh, Thi Lan Anh Luu, Duc Tho Do, Duc Vuong Dang, Huu Lam Nguyen, Hyun Chul Kim, and Cong Tu Nguyen. "Photocatalytic, electrochemical, and electrochromic properties of in situ Ag-decorated WO_3 nanocuboids synthesized via facile hydrothermal method." *Applied Physics A* 128, no. 12 (2022): 1047.

[37] Nguyen, Khoa Dang, Nguyen Quang Thinh Le, Linh Tieu Loan Tieu, Thuy Huong Nguyen, Thi Lan Anh Luu, Huu Hung Nguyen, Cong Tu Nguyen, and Ngoc Phuong Thao Nguyen. "Facile one-step synthesis of in situ WO_3@ Gr nanorods as an efficient material for antimicrobial and decoloration applications." *Advances in Natural Sciences: Nanoscience and Nanotechnology* 15, no. 2 (2024): 025009.

[38] Barbhuiya, Monjur Hassan, Dona Mazumder, Piyush Pandey, and Siddhartha Sankar Dhar. "WO_3@ Bi_2O_3 nanocomposite decorated on N-rGO sheets: A convenient approach to synthesis, characterization, and analysis of their antibacterial behaviour." *Inorganic Chemistry Communications* 173 (2025): 113842.

[39] Cui, Bingbing, Chuanpan Guo, Guodong Fu, and Zhihong Zhang. "Photochromic performance of hydrogel based on deep eutectic solvent induced water soluble Cu-doped WO_3 hybrids with antibacterial property." *Journal of Photochemistry and Photobiology A: Chemistry* 435 (2023): 114320.

[40] Mohamed, Asmaa T., Reda Abdel Hameed, Shahira H. El-Moslamy, Mohamed Fareid, Mohamad Othman, Samah A. Loutfy, Elbadawy A. Kamoun, and Mohamed Elnouby. "Facile synthesis of Fe_2O_3, Fe_2O_3@ CuO and WO_3 nanoparticles: characterization, structure determination and evaluation of their biological activity." *Scientific Reports* 14, no. 1 (2024): 6081.